Supporting Information

High-performance flexible solid-state asymmetric supercapacitor by assembling $NiCo_2S_4$ as cathode and MXene-reduced graphene oxide sponge as anode

Rajeshvari Samatbhai Karmur,[a] Debika Gogoi,[a] Shrishti Sharma,[b] Manash R. Das,[c,d] Anshuman Dalvi,[b] Narendra Nath Ghosh[,a]*

[a] Nano-materials Lab, Department of Chemistry, Birla Institute of Technology and Science, Pilani-K K Birla Goa Campus, Goa-403726, India.

[b] Department of Physics, Birla Institute of Technology and Science Pilani-Pilani Campus, Rajasthan-333031, India.

[c] Advanced Materials Group, Materials Sciences and Technology Division, CSIR-North East Institute of Science and Technology, Jorhat 785006, Assam, India.

[d] Academy of Scientific and Innovative Research (AcSIR), Ghaziabad 201002, India.

*Corresponding author. Tel. /fax: +91 832 2580318/25570339

*E-mail address: naren70@yahoo.com (N. N. Ghosh)

Author's email addresses: p20200051@goa.bits-pilani.ac.in (Rajeshvari Samatbhai Karmur), p20180429@goa.bits-pilani.ac.in (Debika Gogoi), p20190431@pilani.bits-pilani.ac.in (Shrishti Sharma), mnshrdas@yahoo.com (Manash R. Das), adalvi@pilani.bits-pilani.ac.in (Anshuman Dalvi)

S1. Chemical used

Ti_3AlC_2 MAX phase (particle size $\leq$ 200 μm), Lithium Fluoride (LiF), Polyvinylidene difluoride (PVDF), acetylene black, N-methyl-2-pyrrolidinone (NMP), polyvinyl alcohol (PVA), Poly(diallyldimethylammonium chloride) (PDDA), and graphite were purchased from Sigma-Aldrich. Nickel nitrate hexahydrate ($Ni(NO_3)_2.6H_2O$), Cobalt nitrate hexahydrate ($Co(NO_3)_2.6H_2O$), Hydrochloric acid (HCl), ethylene glycol, sodium nitrate ($NaNO_3$), and Potassium permanganate ($KMnO_4$) were purchased from Merck, India. Sulfuric acid (H_2SO_4), Potassium Hydroxide (KOH), Potassium Ferrocyanide ($K_4[Fe(CN)_6]$), Sodium chloride (NaCl), Hydrogen peroxide (H_2O_2), hydrazine hydrate ($NH_2NH_2.H_2O$) and ethanol were purchased from Fisher Scientific. Deionized water was used during the experiments.

S2. Synthesis of Materials

S2.1. Synthesis of $NiCo_2S_4$

The formation of the $NiCo_2S_4$ sphere was carried out using a one-step solvothermal method. Briefly, the 1 mM of $Ni(NO_3)_2.6H_2O$ and 2 mM of $Co(NO_3)_2.6H_2O$ were mixed with the 8 mM of thiourea in the Ethylene glycol and water solution (volume ratio of 1:1) and magnetically stirred the dispersion for 30 min. After that, the dispersion was heated in the stainless-steel autoclave at the temperature of 180ºC for 24 h and naturally cooled down. The final product was washed several times with DI water and ethanol and dried in the oven at 60ºC for 8 h.

S2.2. Synthesis of $Ti_3C_2T_x$ MXene

To synthesize the $Ti_3C_2T_x$ MXene nanosheets, the Ti_3AlC_2 MAX phase was used as precursors and chemically etched to remove the Al layers by using LiF/HCl etchant. In the procedure, the etchant was prepared by adding 0.5 gm LiF to 10 ml of 9 M HCl solution and continuously stirring to dissolve the LiF powder for 5 min. After that, 0.5 gm of Ti_3AlC_2 precursor powder was gradually added to the etching solution and then magnetically stirred at room temperature for 48 h. The final product was collected by centrifuging washing with DI water until the pH value of the supernatant reached $\geq$ 5 and drying at 60ºC for 12 h in the oven.

S2.3. Synthesis of rGO sponge (rGO_{sp})

To synthesize the rGO sponge (rGO_{sp}), initially, a Graphene oxide sponge (GO_{sp}) was prepared from the graphene oxide (GO) by employing a freeze-dried method, and GO was synthesized by using Hummer's method. In the synthesis process of GO, 0.6 g $NaNO_3$ was added to 35 mL conc. H_2SO_4 in a beaker which was kept inside an ice bath. Then 1.3 g of graphite powder was added to the mixture and stirred for 8 h by maintaining the temperature below 5ºC. In that mixture, 3.8 g of $KMnO_4$ was added slowly, and the temperature of the mixture was raised to ~35ºC and stirred for 8-10 h. Then 180 mL of distilled water was added to the mixture, and the

temperature was raised to 98ºC and maintained for ~1 h. After that, 2 mL of 30% H_2O_2 solution was added to the mixture and stirred for 1 h. The obtained product (GO) was washed with 10% HCl solution, distilled water, and ethanol and then dried at 60ºC for 10 h.

In a beaker, GO was well-dispersed in a minimum amount of water and then kept at -80ºC overnight, followed by lyophilization for 72 h. The obtained GO_{sp} was kept in a vacuum oven at 60ºC for 10 h. The prepared GO_{sp} was placed in an alumina crucible with the addition of 6 mL hydrazine hydrate, and then the crucible was covered with a lid. Then it was heated for 3 h at 150ºC to obtain rGO_{sp}.

S2.4 Synthesis of MXene-rGO_{sp} nanocomposite

Synthesized MXene and rGO_{sp} were first prepared by dispersing them separately in methanol during sonication. Then the appropriate amount of these dispersions were mixed in a round-bottomed flask and refluxed for 3 h at 70ºC. MXene-rGO_{sp} nanocomposites with desired compositions were obtained by filtering and drying after refluxing.

S3. Details of Instruments Used

The characterization of synthesized materials employed by using the following characterization techniques: (i) Field emission scanning electron microscopy (FESEM) images of materials were attained using Quanta 250 FEG (FEI), (ii) High-resolution transmission electron microscopy (HRTEM) and selected area electron diffraction (SAED) images were obtained by JEM-2100 (JEOL), 200 kV equipped with LaB_6 filament, (iii) Energy dispersive X-ray spectra (EDS) and elemental mapping was obtained from EDAX ELEMENT electron microscope attached to a Quanta 250 FEG (FEI), (iv) X-ray diffraction (XRD) patterns of the prepared materials were carried out using a powder X-ray diffractometer (Mini Flex II, Rigaku, Japan) with Cu Kα ($\lambda = 0.15405$ nm) radiation at a scanning speed of 3º min^{-1}, (v) Raman spectra were recorded on a Horiba via Raman microscope with a 532 nm laser excitation, (vi) XPS measurements were recorded using a Thermo-Scientific ESCALAB Xi^+ spectrometer having a monochromatic Al Kα X-ray source (1486.6 eV) and a spherical energy analyzer that operate in the CAE (constant analyzer energy) mode, (vii) Fourier Transform Infrared spectra (FTIR) were recorded in KBr by using spectrophotometer (IR Affinity-1, Shimadzu, Japan), (viii) IVIUMSTAT (10V/5A/8MHz) workstation was used to perform all the electrochemical studies.

S4. Electrode Preparation

To fabricate the working cathode and anode electrodes, a mixture of 80 wt% active electrode material, 10 wt% Poly(vinylidene fluoride) in N-methyl-2-pyrrolidinone, and 10 wt% acetylene black was prepared as a homogeneous paste, and then this paste was coated on Ni

foam (1.5 cm × 1.5 cm) and dried at 80C for 24 h under vacuum. The mass loading on the Ni foam was ~ 2 mg. To prepare the electrode for an asymmetric cell, only one side of Ni foam was coated.

The value of specific capacitance (C_S) was calculated by using the following equation:

$$Cs = \frac{i\Delta t}{m\Delta V} \quad \text{(S1)}$$

S5. Design of asymmetric supercapacitor (ASC) cell

The voltammetric charges (Q) were calculated based on the following equations:

$$Q = C_{single} \times \Delta V \times m \quad \text{(S2)}$$

Where C_{single} is the specific capacitance (F g^{-1}), ΔV is the potential window (V), and m is the mass of electrode (g) of each electrode measured in a three-electrode setup.

The charge balance was carried out by the substitution of the above equation for both anode and cathode considering their charge/mass ratio as:

$$\frac{q+}{q-} = \frac{m+}{m-} = \frac{Csp- \times \Delta V-}{Csp+ \times \Delta V+} \quad \text{(S3)}$$

S6. Fabrication of flexible supercapacitor device

To fabricate a flexible device, 30 mL of deionized water was taken in a beaker and heated on a hotplate. 1 g of KOH was added to the boiled water, followed by the gradual addition of 2 g of PVA and stirred till a thick gel was formed. This gel was then pasted between the positive and negative electrodes and allowed to cool and dried at room temperature overnight.

S7. Fabrication 2032 button-type cell

The as-prepared flexible devices were packed in 2032 cell assembly as shown in Fig. 9a. Devices were pressed in a crimper by applying 50 tons/cm^2 of pressure and then used for further characterization.

S8. Equations used to calculate the electrochemical performances

The value energy density (E) and power density (P) for a two-electrode setup were calculated by using the following equations:

$$E = \int_{t1}^{t2} I\,V(t)\,dt \times \frac{1000}{3600} \quad \text{(S4)}$$

$$P = \frac{E}{\Delta t} \times 3600 \quad \text{(S5)}$$

where i denotes the charge or discharge current (A), Δt represents the discharging time (s), m is the mass of electroactive material (g), ΔV is the applied potential window, E is the energy density (W h kg^{-1}), and P is the power density (W kg^{-1}).

The Coulombic efficiency (η) was determined by using the following equation:

$$\eta\,(\%) = \frac{td}{tc} \times 100 \qquad \text{(S6)}$$

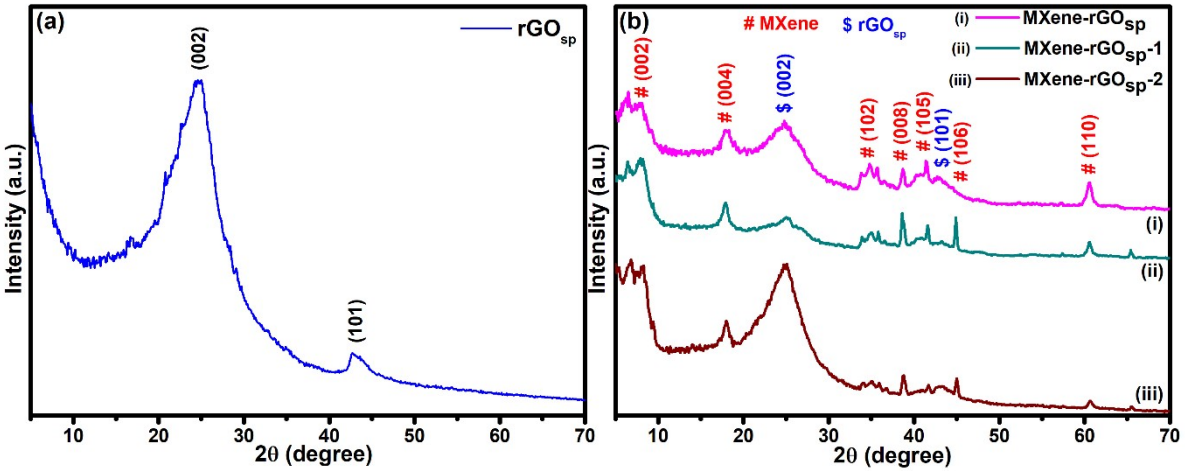

Fig. S1. XRD pattern of (a) pure rGO$_{sp}$, (b) MXene-rGO$_{sp}$ nanocomposites with different wt%.

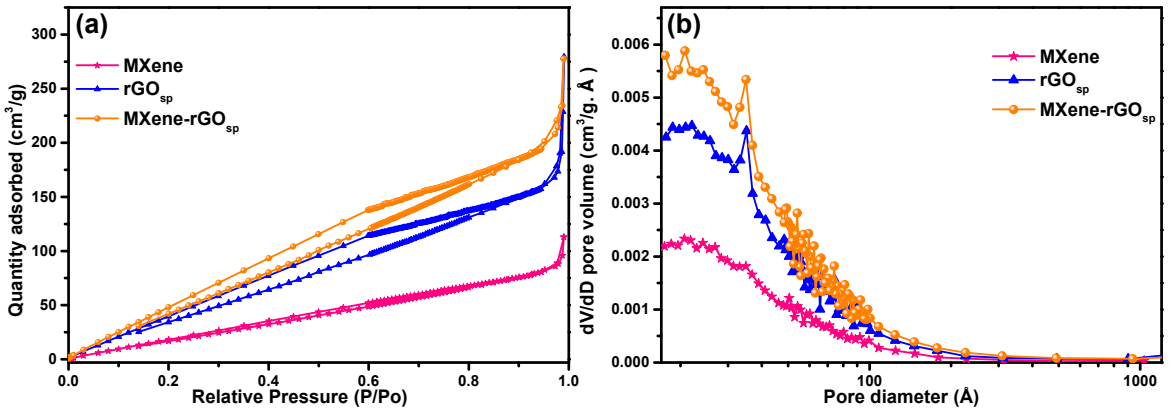

Fig. S2. (a) N_2 adsorption-desorption isotherms and (b) Pore-size distribution plots of MXene, rGO$_{sp}$, and MXene-rGO$_{sp}$ nanocomposite.

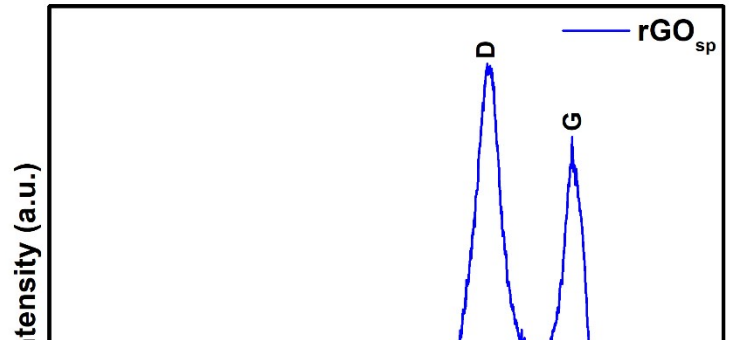

Fig. S3. Raman spectra of pure rGO_{sp}.

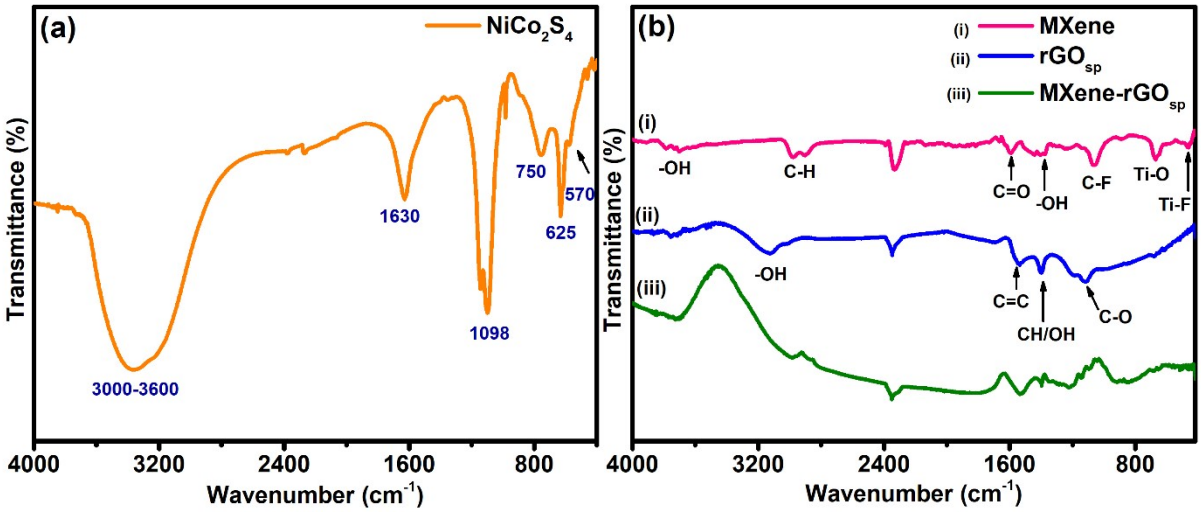

Fig. S4. FTIR spectra of (a) $NiCo_2S_4$, (b) MXene, rGO_{sp}, and MXene-rGO_{sp} nanocomposite.

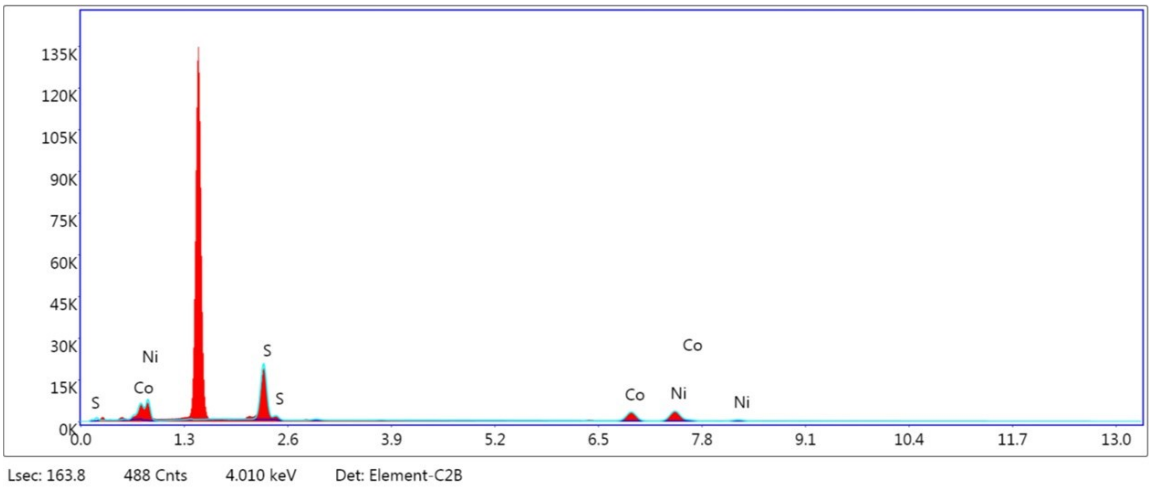

Fig. S5. EDS spectra of $NiCo_2S_4$.

(Note: Al tape was used for sample preparation on stub)

Fig. S6. EDS spectra of MXene-rGO$_{sp}$ nanocomposite.

(Note: Cu tape was used for sample preparation on stub)

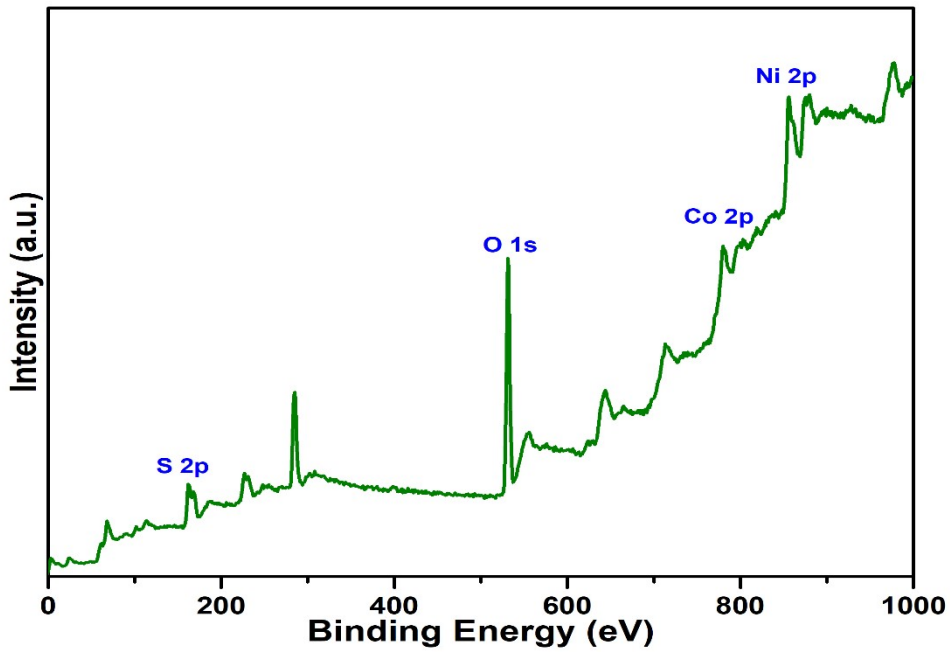

Fig. S7. XPS survey spectrum of $NiCo_2S_4$.

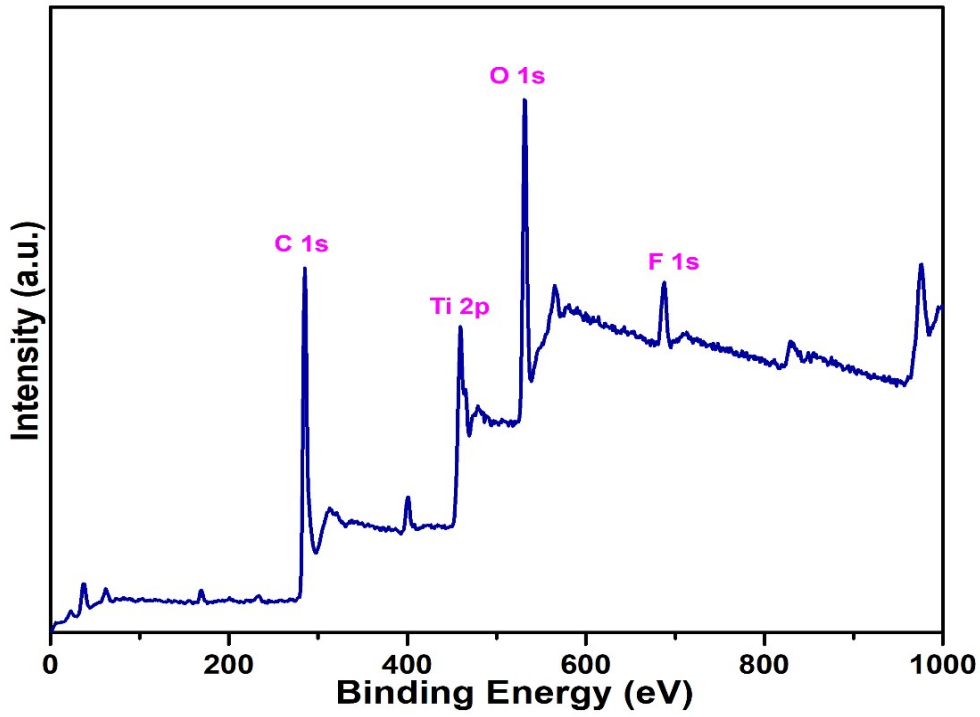

Fig. S8. XPS survey spectrum of MXene-rGO$_{sp}$ nanocomposite.

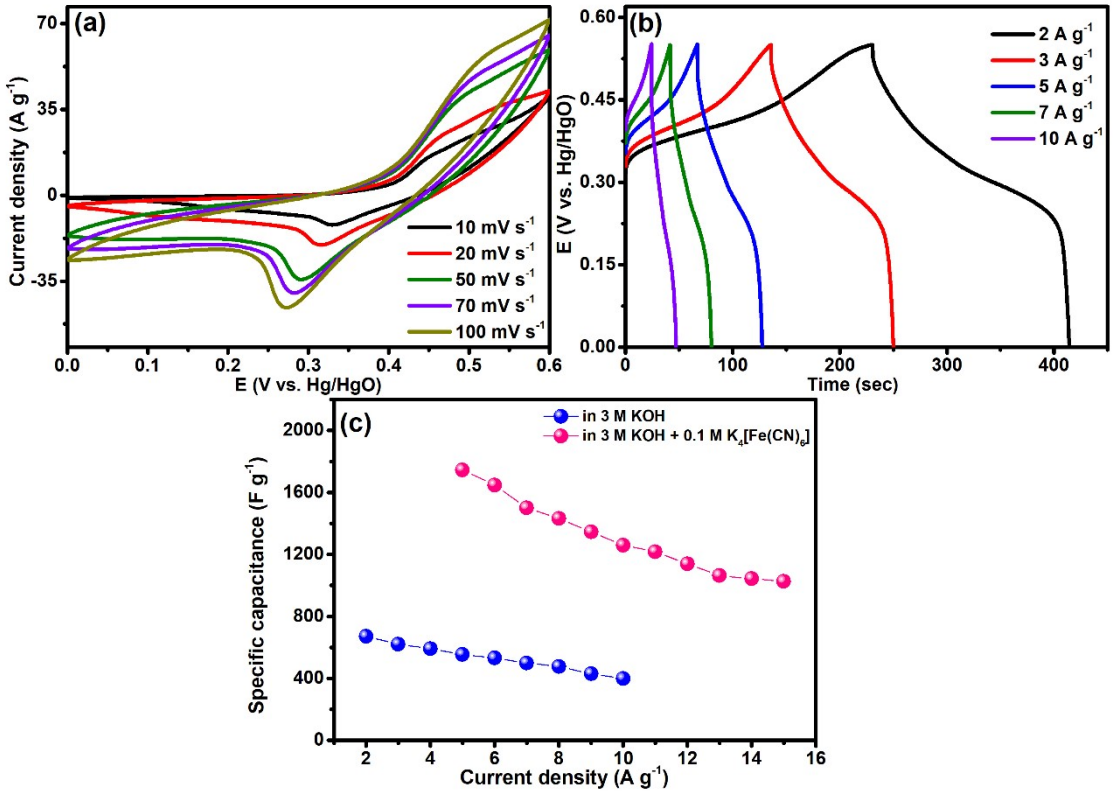

Fig. S9. (a) CV curves at different scan rates and (b) GCD curves at different current densities of $NiCo_2S_4$ in 3 M KOH. (c) Specific capacitance versus scan rate plot of $NiCo_2S_4$.

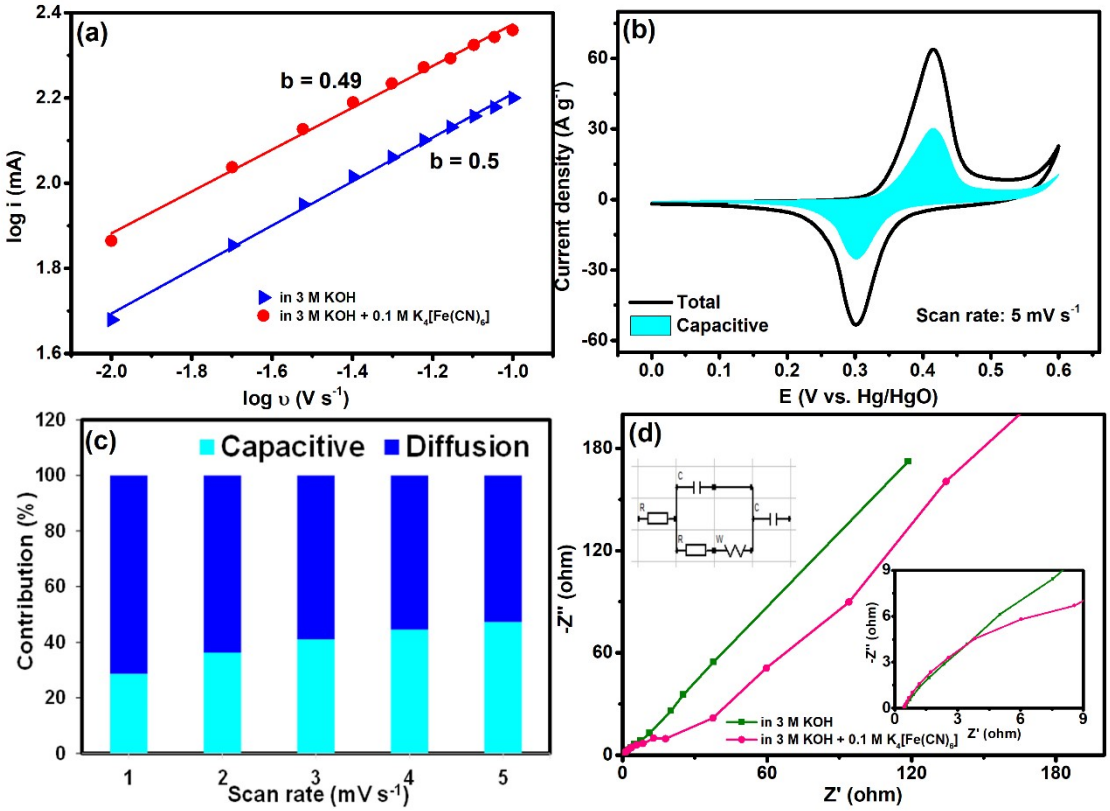

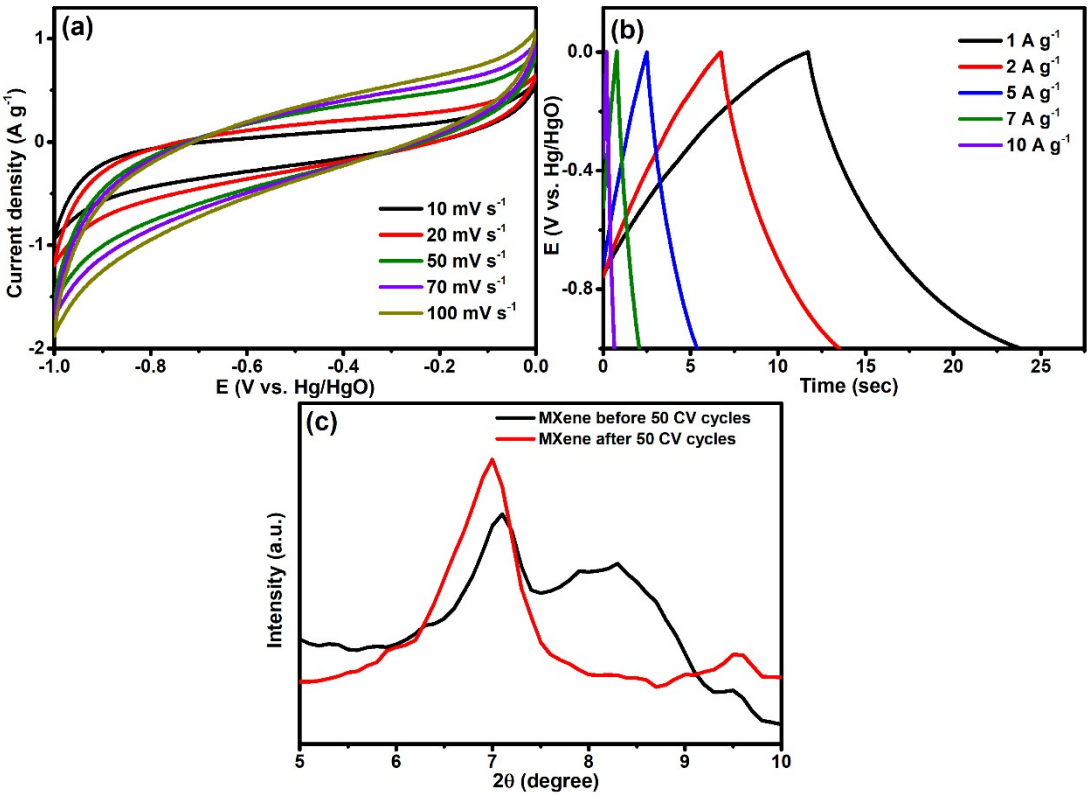

Fig. S11. (a) CV curves at different scan rates and (b) GCD curves at different current densities of MXene in 3 M KOH. (c) XRD pattern of MXene before and after the measurement of 50 CV cycles.

Fig. S10. (a) log i vs. log υ plot, (b) the proportion of capacitive process contributions to the total charge at scan rates of 5 mV s^{-1} in 3 M KOH, (c) the total charge stored on the electrode by both surface capacitive and diffusion-controlled processes at various scan rates in 3 M KOH, and (d) Nyquist plot (inset: used EIS circuit to fit the curve and high-frequency region) of $NiCo_2S_4$.

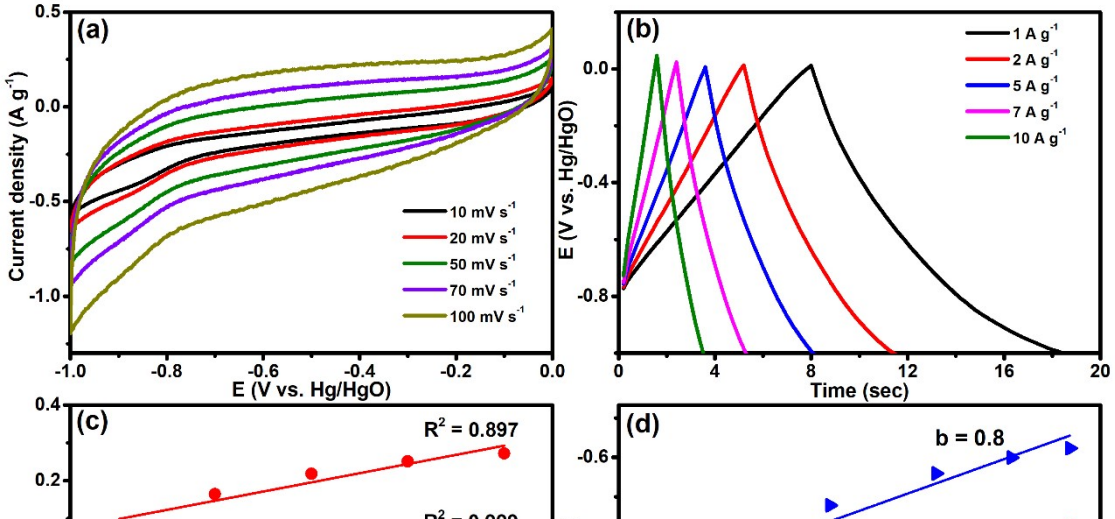

Fig. S12. (a) CV curves at different scan rates and (b) GCD curves at different current densities of MXene in 3 M KOH + 0.1 M $K_4[Fe(CN)_6]$. (c) Randle-Sevcik plot (i vs. υ) and (d) log i vs. log υ plot of MXene.

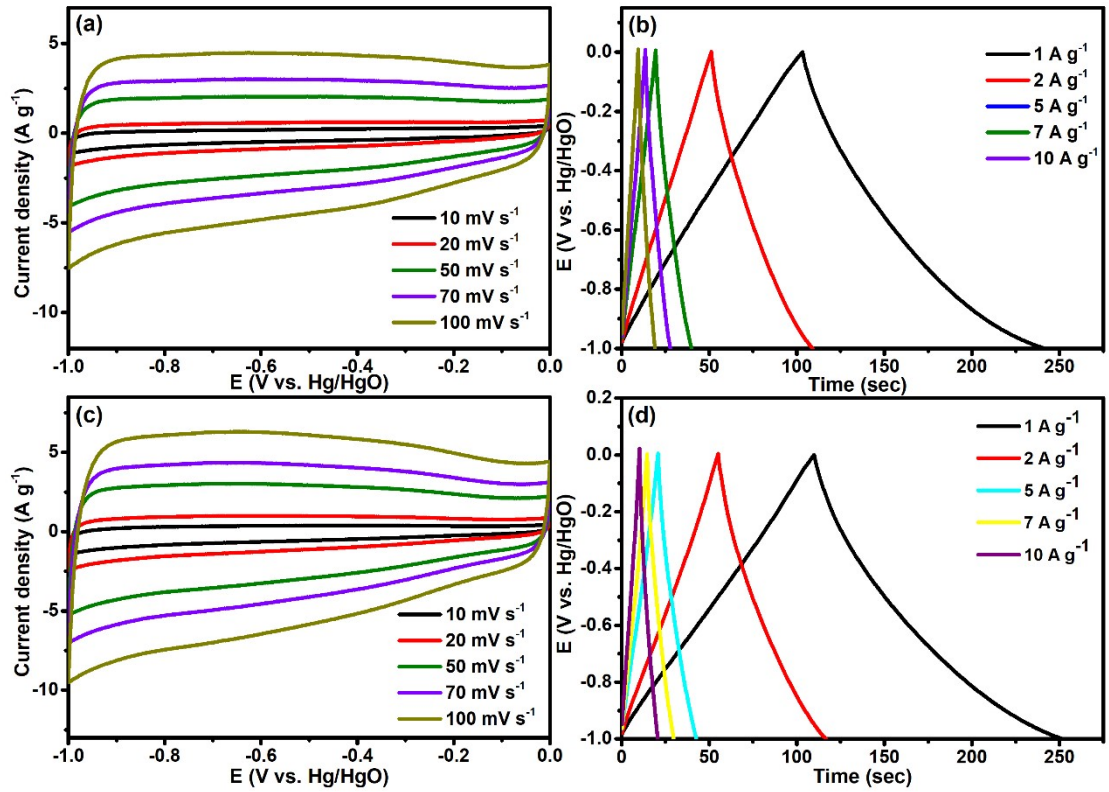

Fig. S13. CV curves at different scan rates and GCD curves at different current densities of rGO_{sp}: (a)-(b) in 3 M KOH and (c)-(d) in 3 M KOH + 0.1 M $K_4[Fe(CN)_6]$.

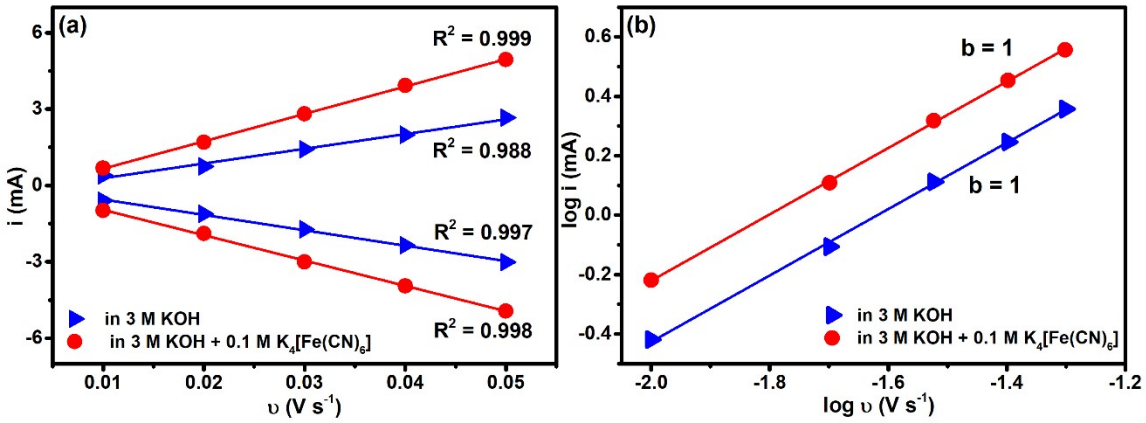

Fig. S14. Randle-Sevcik plots (a) i vs. υ and (b) log i vs. log υ plot of rGO_{sp}.

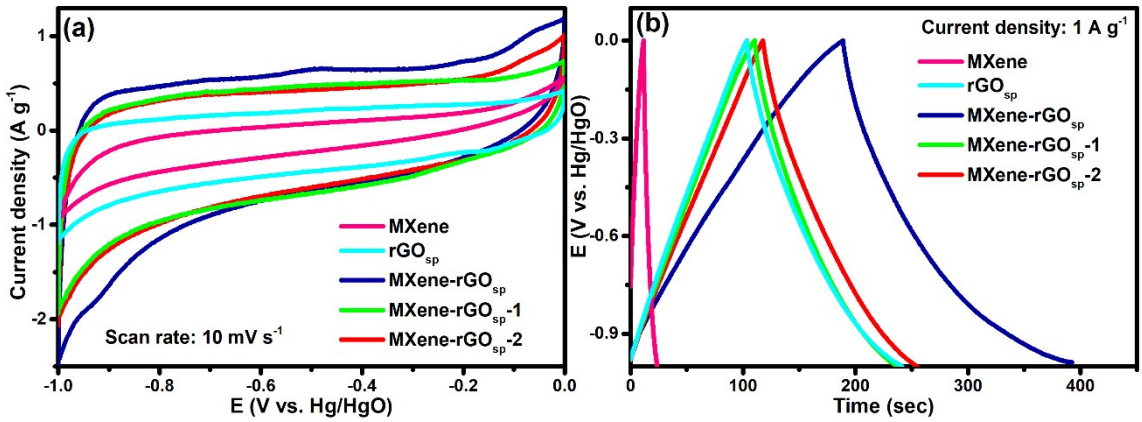

Fig. S15. (a) CV curves at a scan rate of 10 mV s^{-1} and (b) GCD curves at a current density of 1 A g^{-1} of different compositions of MXene-rGO_{sp} nanocomposites in 3 M KOH.

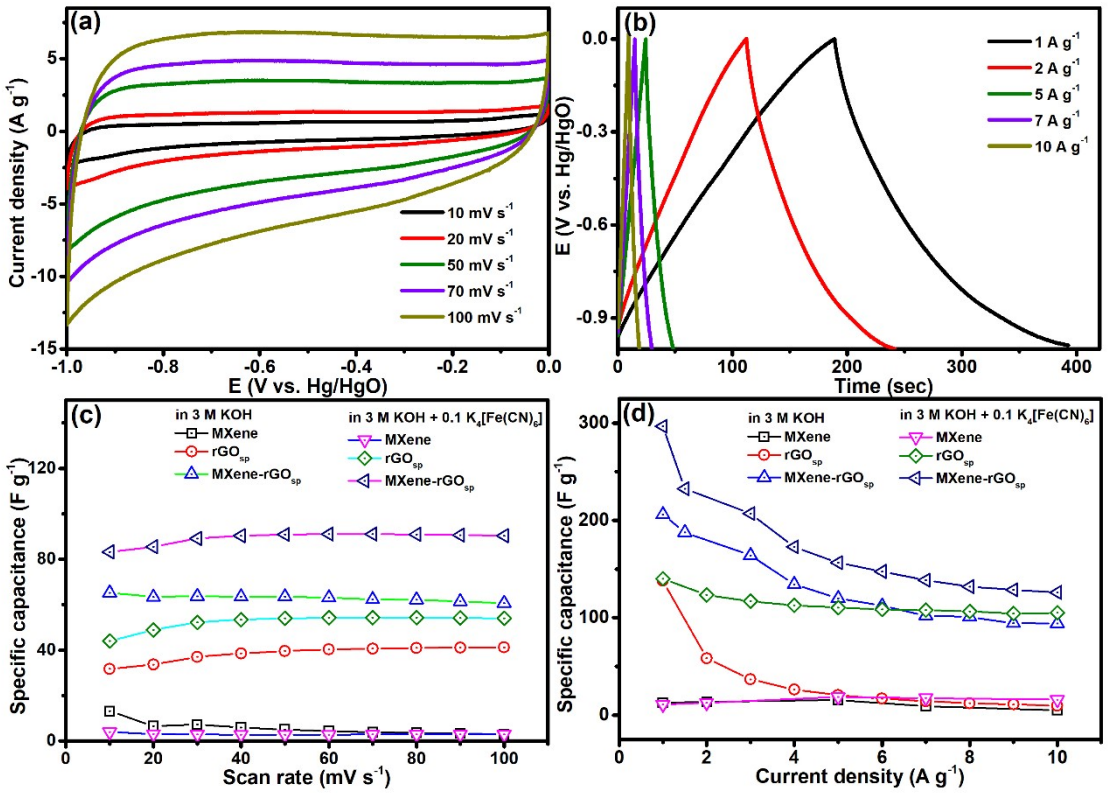

Fig. S16. (a) CV curves at different scan rates and (b) GCD curves at different current densities of MXene-rGO_{sp} in 3 M KOH. (c) Specific capacitance at various scan rates and (d) Specific capacitance at various current densities of MXene, rGO_{sp}, and MXene-rGO_{sp} nanocomposite in 3 M KOH and 3 M KOH + 0.1 M $K_4[Fe(CN)_6]$.

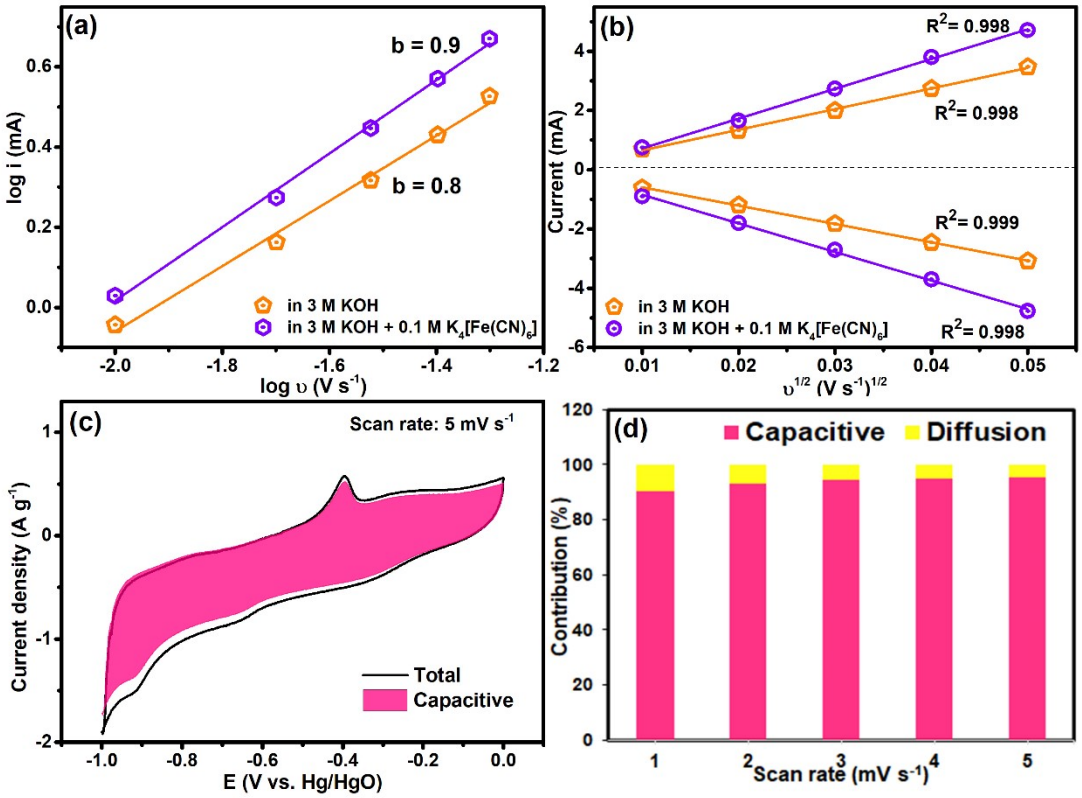

Fig. S17. (a) log i vs. log υ plot, (b) Randle-Sevcik plot, (c) the proportion of capacitive process contributions to the total charge at scan rates of 5 mV s^{-1} in 3 M KOH, and (d) total charge stored on the electrode by both surface capacitive and diffusion-controlled processes at various scan rates in 3 M KOH.

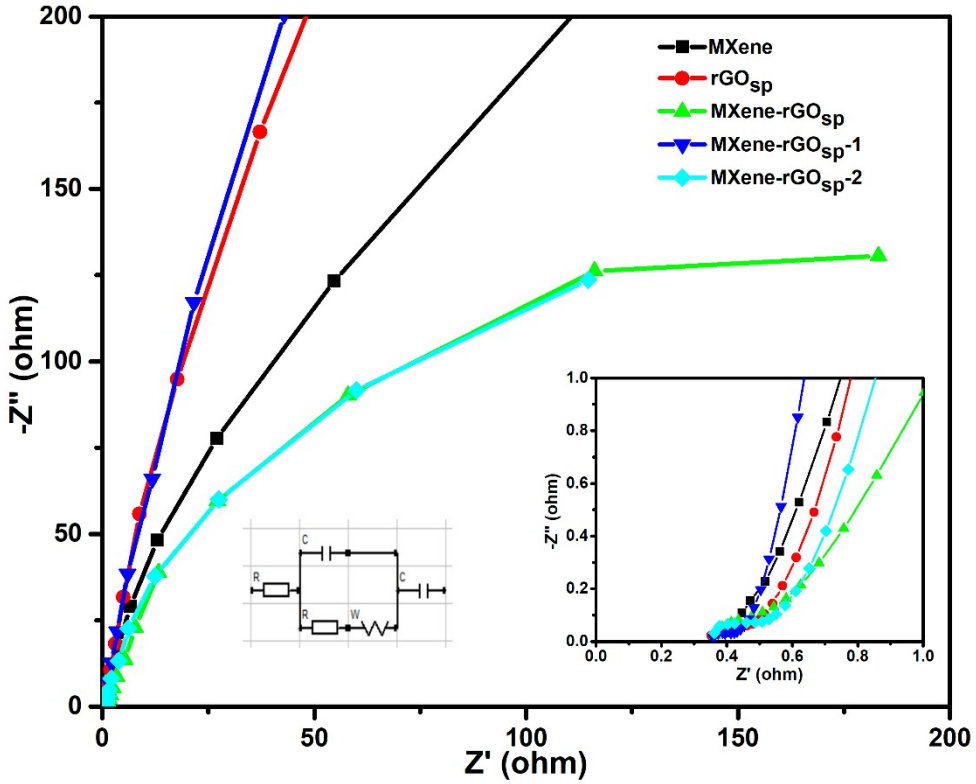

Fig. S18. Nyquist plot of MXene, rGO_{sp}, and different compositions of MXene-rGO_{sp} nanocomposites (inset: EIS circuit used to fit the curve & EIS spectra at high-frequency region).

Table S1. Obtained EIS data of the materials and nanocomposites after the circuit fitting

Sr. No.	Materials	Equivalent Series Resistance (R_1=R_S) Ω	Charge Transfer Resistance (R_2=R_{CT}) Ω
1	MXene	0.47	1.43
2	rGO_{sp}	1.04	1.88
3	MXene-rGO_{sp}	0.43	0.66
4	MXene-rGO_{sp}-1	0.48	1.27
5	MXene-rGO_{sp}-2	0.45	1.71

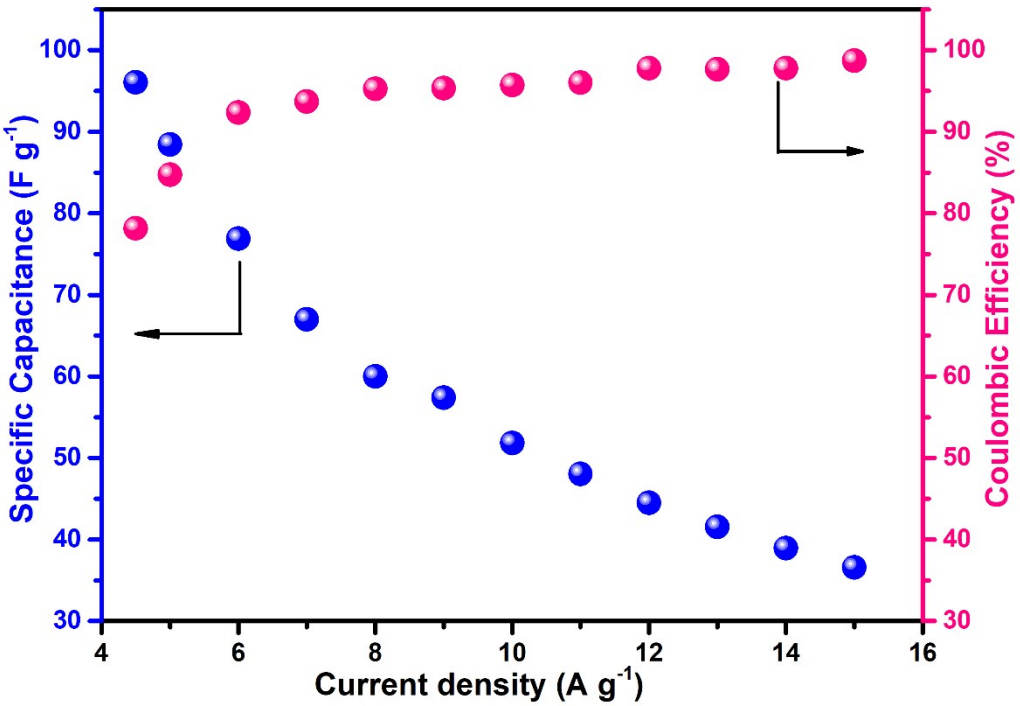

Fig. S19. The change in specific capacitance and Coulombic efficiency (%) with increased current densities.

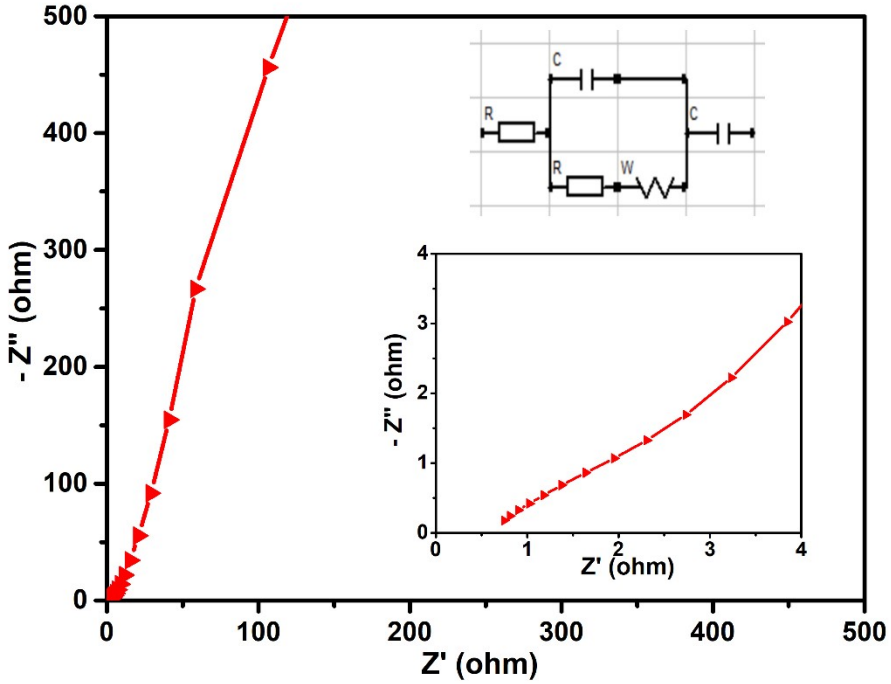

Fig. S20. Nyquist plot of all-solid-state $NiCo_2S_4$//MXene-rGO_{sp} ASC device nanocomposites (inset: EIS circuit used to fit the curve & EIS spectra at high-frequency region).

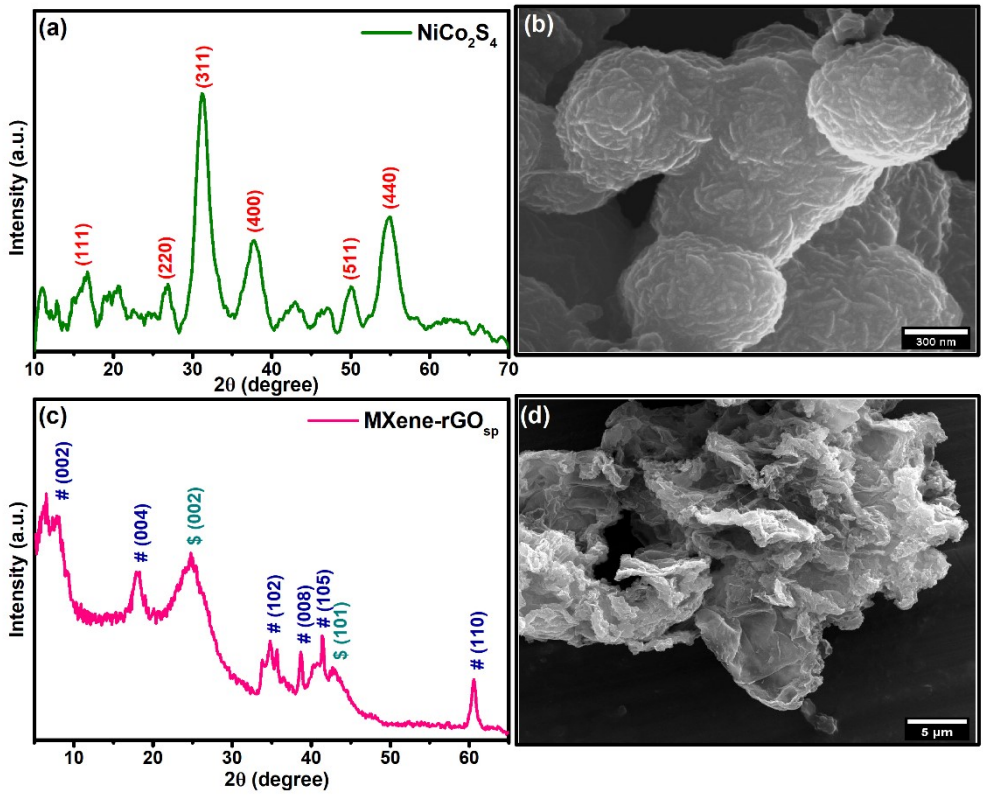

Fig. S21. (a) XRD pattern and (b) FESEM image of $NiCo_2S_4$, and (c) XRD pattern and (b) FESEM image of MXene-rGO_{sp} after 4000 charge-discharge cycles.

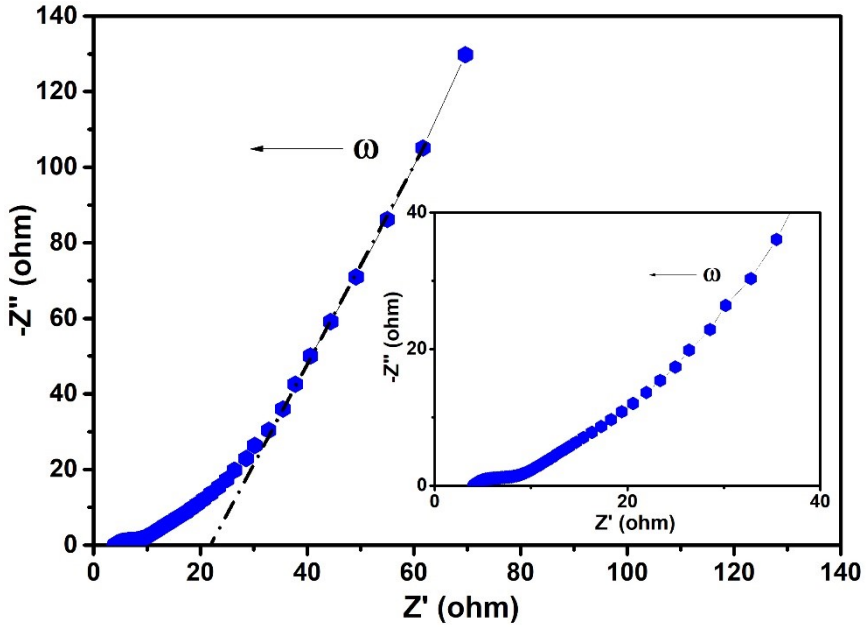

Fig. S22. EIS of 2032 type button cell configuration in the frequency range of 10 MHz to 1MHz.

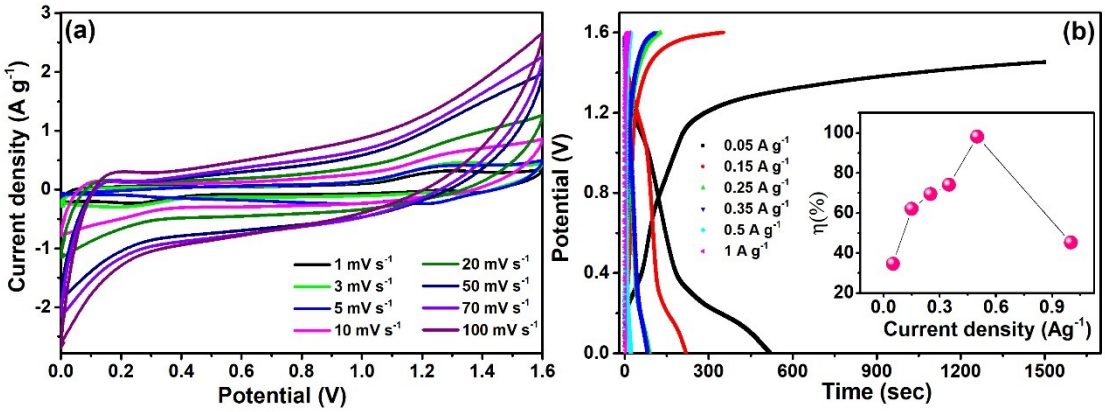

Fig. S23. (a) CV curves at different scan rates, (b) GCD scans at different current densities (inset: Coulombic efficiency plot) of 2032-type cell.

Table S2. Comparison table of the fabricated $NiCo_2S_4$//MXene-rGO_{sp} ASC device (this work) with some of the already reported MXene- based two-electrode supercapacitors.

Sr. No.	Material	Electrolyte	Potential (V)	Energy density	Power density	Retention (cycles)	Ref.

				(W h kg^{-1})	**(W kg^{-1})**		
1.	$Ti_3C_2T_x$-paper//CFP	1 M KOH	1.3	4.5	1300	-	[1]
2.	MLMO//MLMO	3 M KOH	1.6	34.1	795.5	96.2% (10000)	[2]
3.	Ti_3C_2/CuS//Ti_3C_2	1 M KOH	1.5	15.4	750.2	82.4% (5000)	[3]
4.	$Ti_3C_2T_x$//PANI@rGO	3 M H_2SO_4	1.45	17	200	88% (20000)	[4]
5.	RuO_2//$Ti_3C_2T_x$	PVA-H_2SO_4	1.6	29	3800	86% (20000)	[5]
6.	MoS_2/$Ti_3C_2T_x$// MoS_2/$Ti_3C_2T_x$	1 M H_2SO_4	0.6	5.1	298	72.3% (10000)	[6]
7.	$NiCo_2$-LDHs@AL-Ti_3C_2 MXene	6M KOH	1.6	68	388	90% (10000)	[7]
8.	MXene-WO_3@rGO_{sp}//PC	2 M KOH + 0.1M $K_4[Fe(CN)_6]$	1.45	34	1450	86% (3000)	[8]
9.	300-CMC-31:1//AC	PVA + KOH	1.45	10.66	135.96	96.87% (5000)-	[9]
10.	50MXene-50Ni$(OH)_2$//PC	3 M KOH + 0.1M $K_4[Fe(CN)_6]$	1.6	29.3	800	90% (5000)	[10]
11.	MXene/$MoSe_2$//AC	6M KOH	1.6	55.6	800.3	94.1% (10000)	[11]
12.	MnO_2//MXene	PVA/H_2SO_4	1.5	6.4	1107.7	84% (3000)	[12]
13.	Quinolinediol@rGO// MXene	1M H_2SO_4	1.6	27.8	730	83.5% (10000)	[13]
14.	MXene/COS_2(CCH)//	2M KOH	1.6	28.8	800	98%	[14]

	rGO					(5000)	
15.	MXene/NiS//G/AC	2M KOH	2	17.68	750	97.7% (3000)	[15]
16.	$NiCO_2$-LDHs@MXene/rGO// MXene/rGO	2M KOH	1.4	65.3	700	92.8% (10000)	[16]
17.	C3@rGO//$Ti_3C_2T_x$	3M H_2SO_4	1.5	20	480	80% (10000)	[17]
18.	Ti_3C_2Tx−δ-MnO_2//$Ti_3C_2T_x$	1M Na_2SO_4	1.6	8.2	400	-	[18]
19.	d-Ti_3C_2/NF//b-Ti_3C_2	6 M KOH	1.6	18.1	397.8	80.6% (5000)	[19]
20.	MXene/PANI 1:3//AC	7M KOH	2	22.67	217	95.3% (10000)	[20]
21.	$NiCo_2S_4$//MXene-rGO_{sp}	3 M KOH + 0.1M $K_4[Fe(CN)_6]$	1.6	35.75	3693	95% (4000)	**This work**

References

1. W. Wu, S. Lin, T. Chen, L. Li, Y. Pan, M. Zhang, L. Wu, H. Gao and X. Zhang, *J. Alloys Compd.* 2017, **729**, 1165-1171.
2. A. K. Tomar, T. Kshetri, N. H. Kim and J. H. Lee, *Energy Storage Mater.* 2022, **50**, 86-95.
3. Z. Pan, F. Cao, X. Hu and X. Ji, *J. Mater. Chem. A* 2019, **7**, 8984-8992.
4. M. Boota and Y. Gogotsi, *Adv. Energy Mater.* 2019, **9**, 1802917.
5. Q. Jiang, N. Kurra, M. Alhabeb, Y. Gogotsi and H. N. Alshareef, *Adv. Energy Mater.* 2018, **8**, 1703043.
6. W. Hou, Y. Sun, Y. Zhang, T. Wang, L. Wu, Y. Du and W. Zhong, *J. Alloys Compd.* 2021, **859**, 157797.

7. C. Lu, A. Li, T. Zhai, C. Niu, H. Duan, L. Guo and W. Zhou, *Energy Storage Mater.* 2020, **26**, 472-482.

8. R. S. Karmur, D. Gogoi, A. Biswas, C. Prathibha, M. R. Das and N. N. Ghosh, *Appl. Surf. Sci.* 2023, **623**, 157042.

9. L. Liao, A. Zhang, K. Zheng, R. Liu, Y. Cheng, L. Wang, A. Li and J. Liu, *ACS Appl. Mater. Interfaces* 2021, **13**, 28222-28230.

10. R. S. Karmur, D. Gogoi, M. R. Das and N. N. Ghosh, *Energy Fuels* 2022, **36**, 8488-8499.

11. X. Chen, J. Zhu, J. Cai, Y. Zhang and X. Wang, *J. Energy Storage* 2021, **40**, 102721.

12. Y. Wei, M. Zheng, W. Luo, B. Dai, J. Ren, M. Ma, T. Li and Y. Ma, *J. Energy Storage* 2022, **45**, 103715.

13. L. Jiao, F. Ma, X. Wang, Z. Li, Z. Hu and Q. Yin, *ACS Appl. Energy Mater.* 2021, **4**, 7811-7820.

14. H. Liu, R. Hu, J. Qi, Y. Sui, Y. He, Q. Meng, F. Wei, Y. Ren, Y. Zhao and W. Wei, *Adv. Mater. Interfaces* 2020, **7**, 1901659.

15. H. Liu, R. Hu, J. Qi, Y. Sui, Y. He, Q. Meng, F. Wei, Y. Ren and Y. Zhao, *Electrochim. Acta* 2020, **353**, 136526.

16. J. Zheng, X. Pan, X. Huang, D. Xiong, Y. Shang, X. Li, N. Wang, W.-M. Lau and H. Y. Yang, *Chem. Eng. J.* 2020, **396**, 125197.

17. M. Boota, M. Rajesh and M. Bécuwe, *Mater. Today Energy* 2020, **18**, 100532.

18. C. K. Kamaja, S. Mitra, Gaganjot and M. Katiyar, *Energy Fuels* 2022, **36**, 703-709.

19. J. Guo, Y. Zhao, A. liu and T. Ma, *Electrochim. Acta* 2019, **305**, 164-174.

20. Y. Li, P. Kamdem and X.-J. Jin, *J. Alloys Compd.* 2021, **850**, 156608.